Mechanical and structural properties of bone in non-critical and critical healing in rat ☆

Rebecca M. Hoerth [a,b], Britta M. Seidt [a], Miheer Shah [a], Carolin Schwarz [b,c], Bettina M. Willie [c], Georg N. Duda [c], Peter Fratzl [a], Wolfgang Wagermaier [a,*]

[a] Max Planck Institute of Colloids and Interfaces, Department of Biomaterials, Research Campus Golm, 14424 Potsdam, Germany
[b] Berlin-Brandenburg School for Regenerative Therapies (BSRT), Charité – Universitätsmedizin Berlin, Campus Virchow Klinikum, Augustenburger Platz 1, 13353 Berlin, Germany
[c] Julius Wolff Institute & Center for Musculoskeletal Surgery, Charité – Universitätsmedizin Berlin, Campus Virchow Klinikum, Augustenburger Platz 1, 13353 Berlin, Germany

ABSTRACT

A fracture in bone results in a dramatic change of mechanical loading conditions at the site of injury. Usually, bone injuries heal normally but with increasing fracture gaps, healing is retarded, eventually leading to non-unions. The clinical situation of these two processes with different outcomes is well described. However, the exact relation between the mechanical environment and characteristics of the tissues at all levels of structural hierarchy remains unclear. Here we studied the differences in material formation of non-critical (1 mm) and critical (5 mm gap) healing. We employed a rat osteotomy model to explore bone material structure depending upon the different mechanical conditions. In both cases, primary bone formation was followed by secondary bone deposition with mineral particle sizes changing from on average short and thick to long and thin particles. Bony bridging occurred at first in the endosteal callus and the nanostructure and microstructure developed towards cortical ordered material organization. In contrast, in critical healing, instead of bridging, a marrow cavity closure was formed endosteal, exhibiting tissue structure oriented along the curvature and a periosteal callus with less mature material structure. The two healing processes separated between 4 and 6 weeks post-osteotomy. The outcome of healing was determined by the varied geometrical conditions in critical and non-critical healing, inducing completely different mechanical situations.

© 2014 Acta Materialia Inc. Published by Elsevier Ltd. This is an open access article under the CC BY-NC-ND license (http://creativecommons.org/licenses/by-nc-nd/3.0/).

1. Introduction

The capability of bone to structurally adapt to changes of the mechanical environment is based on remodeling of the material [1,2]. Bone is deposited wherever mechanically needed and is resorbed in regions without mechanical need. Bone remodeling can be investigated by changing the mechanical situation of a selected bone and studying the resulting changes in bone mass and structure [1]. Bone regeneration after injury is an extreme situation from a medical perspective which may also change the mechanical environment drastically. In particular, critical defect healing, i.e. the regeneration of a large bone defect, is a well-known and still challenging problem in human orthopedic medicine. Such large defects can result, for example, from resection of large bone parts during cancer treatment or from high-energetic traumatic

events [3]. They often end up in a delayed union or a non-union situation, where a pseudarthrosis is established instead of normally healed bone with restored shape and function.

Injured bone is able to recover from damage [4–6] in a very complex, but also highly coordinated process [6], undergoing changes in composition, structure and mechanical properties. Several successive stages can be distinguished in secondary bone healing [5–7]: an inflammatory phase is followed by intramembranous woven bone deposition far away from the fracture site and cartilage callus formation near the fracture, which later ossifies [4,5,7]. This primary bone gets remodeled and replaced by lamellar bone and redundant callus tissue gets resorbed [4], leading to restoration of shape, functionality and properties. This two-wave process was, for example, shown in a sheep osteotomy model [8]. From a mechano-biological point of view, healing depends especially on the mechanical stimulation of the tissue [9] and of the cells [10] around the fracture gap. The establishment of a bony bridge protects the still fragile tissue within the fracture gap from high stresses by transferring load across the gap, enabling further endochondral ossification [11]. Hence, the formation and

---

differentiation of different callus tissues strongly depends on the loading history [12].

Indeed, bone and callus are hierarchically structured materials and their properties depend on structural features from the millimeter to the nanometer range. The nanometer range consists of carbonated hydroxyapatite platelets and an organic collagen matrix, building up mineralized collagen fibers, the basic building blocks [13,14]. Only a few studies have taken into account the mechanical and nanostructural properties of the bone material itself. Although the clinical situation of healing is well described, the differences between bone material in critical and non-critical healing with regard to the different loading conditions have not yet been addressed.

In this study, we investigate a rat femoral osteotomy model with different gap sizes at different time points during healing. In earlier publications from the underlying study, 1 and 5 mm osteotomies were histologically analyzed (6 and 8 weeks post-osteotomy) by means of differences in tissue composition between both groups [15]. The reproducibility of the atrophic non-union with a prolapse of surrounding soft tissue into the defect and the formation of a bony closure of the marrow cavity was described, for the critical healing model [15]. Furthermore, these osteotomies were analyzed for bony callus formation, patterning and mineralization. The experimental data were combined with finite element analysis, based on micro-computed tomography (μCT) data (2, 4 and 6 weeks post-osteotomy) [16]. It was observed that early mechanical stimuli crucially influence callus patterning [16]. In consequence, with this osteotomy model we found a perfectly suited way to investigate the influence of a bony bridging on the characteristics of the bony tissue and the healing outcome. 1 and 5 mm femur osteotomies were externally fixed and left empty (i.e. no grafts, scaffolds or growth factor treatments) so that the actual gap size is the only difference between the two situations. The bony bridging in the non-critical healing situation alters the mechanical environment dramatically.

In the present study, we aimed at identifying when and to what degree tissue structure and organization diverge between the two healing process. We characterized the changes in compositional, mechanical and structural properties using environmental scanning electron microscopy (ESEM) with backscattered electron imaging (BSE), nanoindentation (NI) and scanning small- and wide-angle X-ray scattering and diffraction (SAXS/WAXD). By comparing the nanoscale architecture of bone material during healing, we propose a model where the same processes at the material scale lead to both scenarios, a regenerated bone in non-critical healing and a non-union in critical healing, just because of different geometric constraints.

2. Materials and methods

2.1. Sample preparation

Externally fixed non-critical healing and critical size femoral osteotomy models, defined by the osteotomy gap size (1 and 5 mm, respectively) were investigated and therefore 16 Sprague Dawley rats (12 weeks old, weight 250–300 g, Charles River Deutschland GmbH, Sulzfeld, Germany) were separated in two groups of eight animals each. The operative procedure has been previously reported [15,17]; for more details see Supplementary Information. All animal experiments were carried out according to the policies and procedures approved by the local legal representative (LAGeSo Berlin, G0071/07). After 2, 3, 4 and 6 weeks of healing, two animals per group were sacrificed by intracardiac potassium chloride injection, while under deep anesthesia. The osteotomized and contralateral femurs were harvested and subsequently fixed in 10%

formalin, dehydrated in ascending grades of ethanol and then put in Xylol. The samples were embedded in methylmethacrylate (MMA; Technovit® 9100 new). We denote the non-critical healing samples with N and the critical size defect samples with C, indicate the number of weeks post-osteotomy with a number and specify the first and the second sample with I or II (e.g. the 2 weeks non-critical healing first sample is named N2I; see Supplementary Information, Table S.1).

2.2. ESEM/BSE

For characterizations with an environmental scanning electron microscope, the embedded samples were cut with a low-speed diamond saw (Buehler Isomet, Buehler GmbH, Duesseldorf, Germany) in a longitudinal direction and polished. ESEM (FEI Company, Oregon, USA) with a backscattered electron detector at 200- or 250-fold magnification was performed. An acceleration voltage of 10 or 12.5 kV, a working distance of ~10 mm and a low vacuum environment (0.75 Torr) were used for the measurements. Single images were then put together using the software provided with the device and Photoshop CS5 (Adobe Systems, Munich, Germany). ESEM/BSE images give information about the mineralization of the analyzed tissue. Brighter grey values signify qualitatively higher calcium content as Ca is the element with the highest atomic number present within the tissue [18].

2.3. NI

NI experiments were performed to investigate the mechanical properties of the newly formed bone compared to those of preexisting cortical bone within two C6 samples and one N6 sample, see also Table S.1. Scanning NI measurements were conducted with a NI device (Hysitron Inc., Minneapolis, USA) using a Berkovich diamond indenter tip. The sample was cut as a block and polished to obtain a smooth and plane-parallel surface (PM5, Logitech, Glasgow, UK, using diamond spray, grain size 0.25 μm) and then mounted on the sample stage. To better understand the healing outcome, the mechanical properties were evaluated for several specific regions: the middle and the outer cortex, the callus in the outer, the middle part or adjacent to the cortex, the callus near the osteotomy or in the osteotomy and for the critical healing samples the callus of the closure (Table 1). The evaluated area was ~100 μm × 200 μm per region, consisting of 11 × 21 measurement points, with a step size of 10 μm (for an exact number of indents, see Table 1). The measurement procedure was described previously [19]. Briefly, the starting point of the measurement was specified using a light microscope. The scanning measurement and the approaching of the indenter tip towards the sample were performed using a Triboscanner. The loading of each indentation consisted of a first loading phase (loading rate 1000 μN s^{-1}), a first resting phase (loading 5000 μN for 60 s), a first unloading phase (unloading rate 400 μN s^{-1}), a second resting phase (1000 μN for 10 s) and a second unloading phase (unloading rate 200 μN s^{-1}). Hardness H and indentation modulus E_r were calculated as described before [19] and measurement points with indentation moduli below a threshold of 10 GPa were excluded, since they were attributed to the embedding material or next to holes within the bone. Mean values and standard deviations were determined for all the regions and given as mean values and standard deviations in Table 1.

2.4. SAXS

Longitudinal sample sections were ground down to a thickness of ~200 μm by hand using 1200 silicon carbide grinding paper (grain size 15 μm). The samples were mounted on a motorized
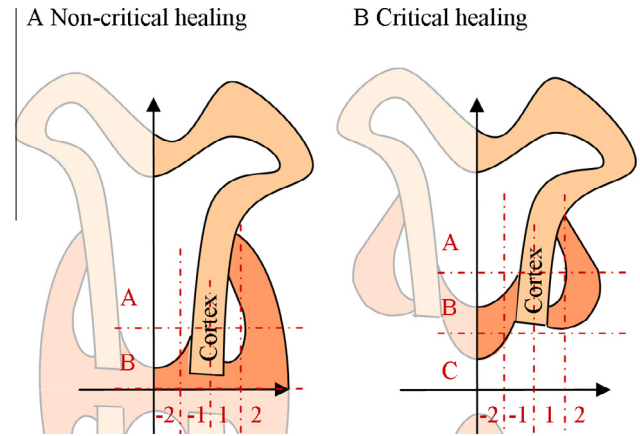
Table 1
Results of NI experiments (indentation modulus and hardness are given as mean ± standard deviation).

Samples	Region	Number of indents	Indentation modulus E_r [GPa] (mean ± SD)	Hardness H [GPa] (mean ± SD)
N6II	Middle cortex	231	22.8 ± 3.7	0.9 ± 0.2
	Adjacent callus	187	22.0 ± 4.6	0.9 ± 0.3
	Callus near osteotomy	231	20.3 ± 3.0	0.8 ± 0.2
	Callus in osteotomy	208	19.8 ± 3.7	0.8 ± 0.2
	Middle cortex near osteotomy	208	22.7 ± 3.2	1.0 ± 0.2
C6I	Outer cortex	231	28.3 ± 3.4	1.3 ± 0.2
	Adjacent callus	231	22.7 ± 3.1	1.0 ± 0.2
	Outer callus	231	16.9 ± 3.2	0.7 ± 0.2
	Callus in osteotomy	231	23.1 ± 3.9	1.0 ± 0.2
	Middle cortex near osteotomy	121	22.7 ± 3.6	1.1 ± 0.2
	Closure	121	16.7 ± 3.3	0.8 ± 0.2
C6II	Middle cortex	231	20.9 ± 3.1	0.9 ± 0.2
	Adjacent callus	231	19.0 ± 2.3	0.8 ± 0.1
	Outer cortex	231	25.5 ± 4.4	1.1 ± 0.2
	Middle callus	231	19.3 ± 2.3	0.7 ± 0.1
	Closure	231	18.9 ± 3.3	0.7 ± 0.2

Fig. 1. Different areas of the callus tissue for evaluation of SAXS measurements. Taking the center of the osteotomy as the origin, the longitudinal sections were divided into four quadrants. Choosing the cortex as a reference, the callus of every quadrant was defined in eight areas that were defined on the distance to the osteotomy (vertical direction A and B), the distance from the cortex and the side of the cortex (horizontal direction, −2, −1, 1 and 2). For the critical size osteotomy model (panel B), a ninth area, the site of closure of the marrow canal (the whole row C) was added.

sample holder to scan the sample perpendicular to the X-ray beam path with a sample-to-detector distance of ~600 mm. The X-ray generator (Bruker, AXS, Karlsruhe, Germany) with a rotating copper anode operating at 40 kV and 100 mA (Cu K_α radiation) produced a beam with a wavelength of 1.54 Å, which was collimated to a diameter of 200 μm by a two-pinhole setup. A radiograph, measuring the transmission with a diode in a spatially resolved way, was performed in order to specify the measurement points for the subsequent scattering experiment. The pre-assigned points (within mineralized area, 200 μm step size) were irradiated during 3600 s and the scattered X-rays (shielding the direct beam with a beam stop) were recorded with a position sensitive area detector (HI-STAR, Bruker AXS, Karlsruhe, Germany, pixel size 105.3 μm × 105.3 μm). The calibration was done with silver behenate. The scattering data were then analyzed with AutoFit custom-made software (Max Planck Institute of Colloids and Interfaces, Potsdam, Germany). Briefly, using the SAXS signal, two different parameters were determined: the T parameter describes the mean thickness of the platelet-shaped mineral particles and its definition is $T = \frac{4\Phi(1 - \Phi)}{\sigma}$, with total volume fraction Φ and total surface area σ of the hydroxyapatite particles [13,20]. It was calculated from a radial SAXS intensity profile to give the mean thickness of the hydroxyapatite platelets of the irradiated bone volume [21]. The direction of the predominant orientation of the mineral platelets and the ρ parameter, describing the degree of orientation (ρ = 0 means no predominant orientation and ρ = 1 means that the platelets are fully aligned), was obtained using an azimuthal intensity profile [21]. By mapping the entire samples, structure and orientation of the bone tissue at the nanometer scale were visualized.

2.5. SAXS data evaluation

To better evaluate the data and to be able to detect gradients with respect to the distance to the cortex and to the osteotomy, the callus tissue of the longitudinal sections was divided into different areas (see Fig. 1). Briefly, taking the center of the osteotomy as the origin, the sample was split into four quadrants and each quadrant was then intersected into different areas. Therefore the

cortex area was identified easily using the SAXS results images with the ESEM/BSE images in the background (see also Figs. 2 and 4). Taking the cortex as a reference, the callus tissue of every quadrant was sectioned into eight areas, depending on the distance to the osteotomy site, the distance to the cortex and the side of the cortex. Thus, the areas were called B if they were more than 800 μm away from the osteotomy and A if not. The areas were called −2 if they were more and −1 if they were less than 400 μm away from the endosteal side of the cortex and 1 and 2 if they were less or more than 200 μm from the periosteal side of the cortex. Therefore, the eight areas were named A−2, A−1, A1, A2, B−2, B−1, B1 and B2 (see Fig. 1). For the critical size osteotomy samples, everything that was within the osteotomy gap and farther away from the cortex cutting edge than 200 μm was included in an additional ninth area (C, see Fig. 1).

2.6. SAXS and WAXD using synchrotron radiation

To enable high resolution analysis in selected regions of interest, further experiments were performed using the synchrotron X-ray source at the μSpot beamline at BESSY II (Berliner Elektronenspeicherring-Gesellschaft für Synchrotronstrahlung, Helmholtz-Zentrum Berlin, Germany). Therefore, samples were ground by hand using 1200 grinding paper to obtain slices with a thickness of ~70 μm and then clamped between aluminum frames to mount them perpendicular to the X-ray beam path at a distance of 300 mm to the detector. A silicon 111 monochromator was used to obtain a monochrome X-ray beam with a wavelength of 0.83 Å. The beam was focused and collimated to a beam size of 30 μm using a two-pinhole setup. Calibration was done using a quartz standard. The scattering patterns were detected during an exposure time of 80–180 s (depending on the mineralization of the tissue) with a position sensitive CCD-detector with a pixel size of 73.2 μm × 73.2 μm (MarMosaic 225, Mar USA Evanston, USA). Results were evaluated and analyzed using AutoFit. ρ and T parameters were calculated as described above.

An additional parameter was determined from the WAXD signal; the L parameter, which is related to the mean mineral crystal length. The definition of the L parameter is $L = \frac{k\lambda}{B\cos\theta}$, with the wavelength λ, the Bragg angle θ and a constant k [22,23]. The full width at half maximum intensity of the (002) peak from crystalline
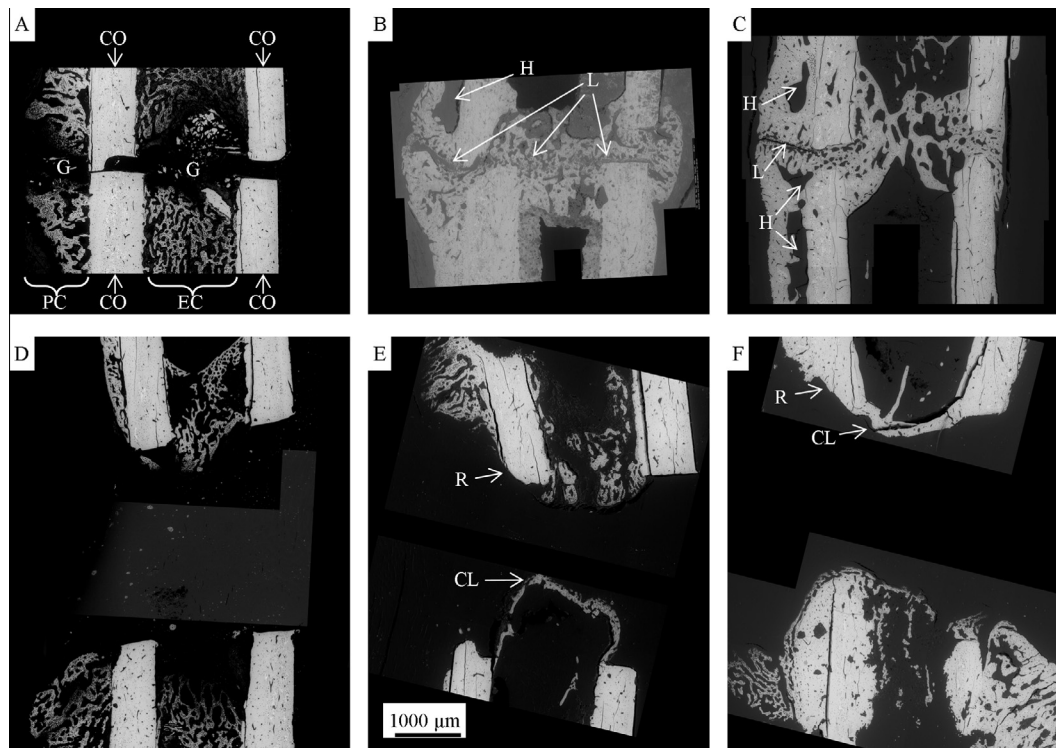
Fig. 2. ESEM/BSE images of non-critical and critical size defect healing process at different time points. In (A), cortices are marked CO, periosteal and endosteal callus areas with PC and EC, respectively. The external fixator was introduced from lateral (right side of the images). (A–C) Non-critical healing samples 2, 4, and 6 weeks post-osteotomy. (D–F) Critical healing samples at the same time points. In (A), large gaps with non-mineralized and less mineralized tissue between the proximal and distal osteotomy fragments, mainly filled with cartilage tissue (see Fig. S.2) are marked G. (There are some small fragments of former cortex left within the gap in the marrow cavity.). In (B, C), L marks the remaining separating line, where the proximal and distal callus got in contact, consisting of cartilage remnants (compare Fig. S.2). In contrast, the big holes (marked H in (B, C) within the periosteal callus, located adjacent to the cortex, were filled with marrow tissue (see Fig. S.2). In (E, F), CL highlights the bony callus tissue that closed off the marrow cavity and R the rounding of the cortices.
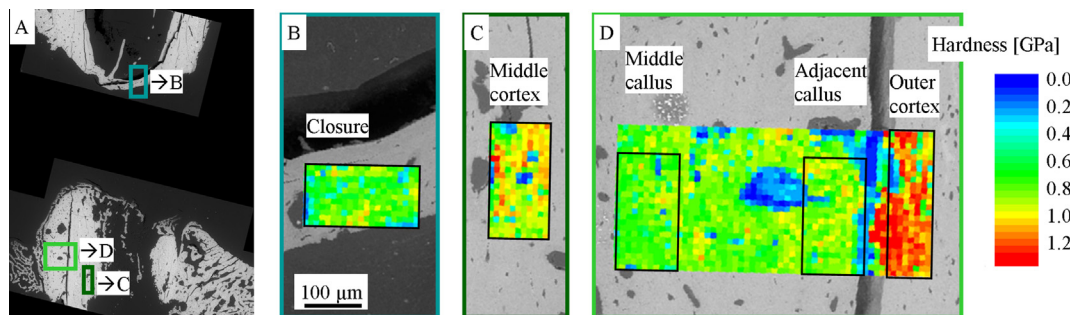
Fig. 3. Hardness maps of selected areas within the closure (B), the middle cortex (C), the middle (periosteal) callus, the adjacent (periosteal) callus and the outer cortex (D) (values, see Table 1, C6II).

hydroxyapatite, defined as *B*, was determined from a radial intensity profile and was used to calculate the *L* parameter through the Scherrer equation [24]. However, the calculation of the *L* parameter did not include corrections for microstrain effects, which would be needed for an exact mineral crystal length determination [25], but enabled a relative comparison between regions with different mean crystal lengths.

Calculations during the analysis and the determinations of the parameters, as well as the statistical calculations, were performed using SigmaPlot 11 (Systat Software) for both, NI and X-ray scattering experiments. Visualization and color mapping was done in Origin 8G (OriginLab, Northampton, USA). Further visualization and combination of different methods were performed with Photoshop CS5 (Adobe Systems, Munich, Germany).

3. Results

3.1. Morphology and mineralization of the tissue

The ESEM/BSE was performed to obtain an overview of the mineralization state of the newly formed callus and the size of the remaining gap. It was possible to distinguish between rather loose, unstructured primary bone and dense, lamellar-structured secondary bone, so we used ESEM/BSE to specifically describe the bone morphology (Fig. 2). At 2 weeks post-osteotomy, healing was characterized by large volumes of periosteal and endosteal primary bony callus formation (Fig. 2A, marked PC). The periosteal bone callus of the N2 sample had a loose appearance including a large volume with finger-shaped primary bone parts. The endosteal

callus consisted of loose primary bone, filling the marrow cavity near the osteotomy site (Fig. 2A, marked EC). Between the periosteal and endosteal callus of the opposing osteotomy ends, areas of less mineralized tissue were found (Fig. 2A, marked G). At 4 weeks post-osteotomy, increased bone formation occurred both periosteal and endosteal with a remaining line of cartilage along the entire length of the original osteotomy (Fig. 2B and Supplementary Information, Fig. S.2B, in both marked L). The bony callus had a lamellar structure, gaining in compactness and thereby the endosteal callus closed off the marrow cavity. In the N6, only the medial periosteal callus still revealed this remaining line (L), while the endosteal and lateral callus sites were characterized by advanced healing with bony bridging. Additionally, the periosteal callus contained large bone marrow filled holes, adjacent to the cortex (marked H, Figs. 2B and C and S.2B and C).

Similar callus formation was detected in the critical size defects. The periosteal and endosteal callus revealed primary bone formation that was later concentrated to the osteotomy site. Especially the endosteal callus penetrated deeply into the defect site, resulting in an arc-like shaped bony callus between the cortices of each osteotomy fragment, which closed off the marrow cavity. A narrowing of the gap due to this arc formation was detectable (Fig. 2D–F), but obviously did not result in thin line that later disappeared (compare Fig. 2A and B, marked G and L). The closure of the marrow cavity had a dense morphology (Fig. 2F) and consisted of lamellar bone, but only one side of the osteotomy fragment demonstrated such a compact closure, while the other side showed primary bone. Hence, instead of fusing to form one endosteal callus plate, intersecting the medullary canal (as during non-critical healing), the two opposing callus parts were still far from each other and formed two closures of the marrow cavity. Moreover, with advanced healing in the critical size osteotomy, the cortical ends revealed a rounding of the edges (Fig. 2E and F, marked R).

3.2. Mechanical properties

Looking first at the middle cortex values as a reference, the distance to the osteotomy site did not affect NI outcome measures within the cortex. The indentation modulus (Table 1) and hardness values were similar for the cortex near to and far from the osteotomy gap. The values were in the same range for the non-critical and the critical size defect. The values for the outer cortex part were higher than the middle cortex values (Fig. 3C and D, and Table 1). When examining only the newly formed bone tissue, the values decreased with decreasing distance to the osteotomy and the values further decreased for the callus within the osteotomy site. The same trend occurred with increasing distance to the preexisting cortex. For the closure of the marrow cavity, the values were always lower than in the middle cortex and in the range of the other callus values (Fig. 3B and C and Table 1).

3.3. Mineral particle orientation

3.3.1. Predominant orientation

The degree of orientation (ρ parameter) and the predominant orientation give important information on the maturity and the structure of the newly formed bone and undergo continuous changes. In the N2 sample, the bony callus was oriented outwards and to the outer side of the callus at the osteotomy site. Yet, the outwards orientation was not true for the C2 sample. For the N6 sample, there was no loose primary bone tissue left but the ρ parameter values were still lower than in the cortex (Fig. 4B and F). The orientation of the bony callus was parallel to the cortex orientation and the long axis of the bone. With decreasing distance to the osteotomy site, the orientation led slightly outwards and then turned into the gap, when reaching the osteotomy. Within the osteotomy gap, the direction was horizontal, thus perpendicular to the long axis of the bone. This inwards orientation and the horizontal alignment within the intracortical gap were located at the contact line between the opposing osteotomy fragments, getting in contact with each other (compare Fig. 2B and C, marked L). In the C6 sample, primary and secondary bone was still present. The remaining loose primary callus (distal osteotomy part, outer medial callus tissue) showed low ρ parameter values and was still oriented outwards in a diagonal way (Fig. 4D and H). The dense inner callus part was oriented along the cortex and the long axis of the bone, and turned inwards, when the osteotomy site was reached. The endosteal callus of the 6 week samples seemed already to be well oriented. However, the predominant orientation in the N6 sample was in the vertical direction (parallel to the long
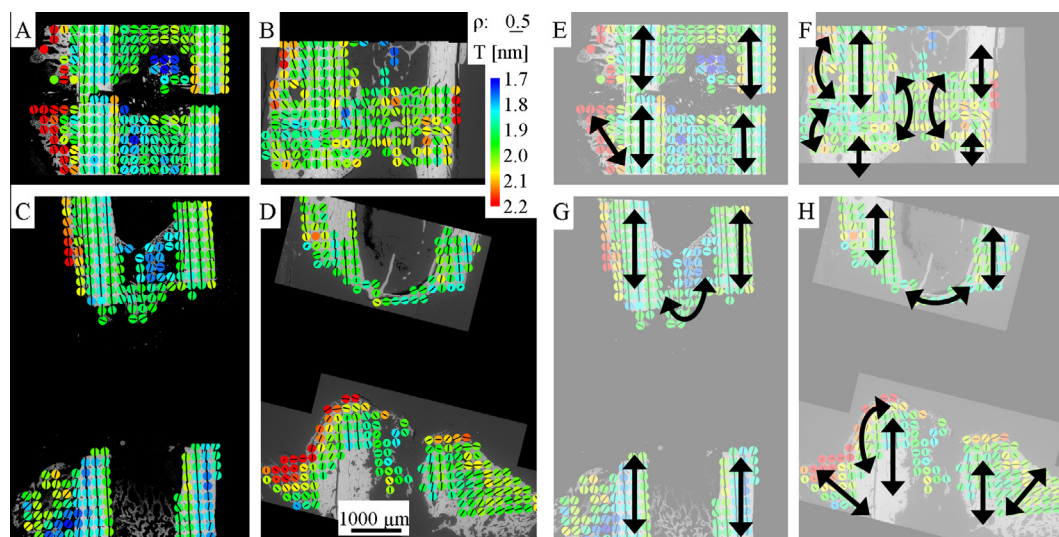
Fig. 4. Results of SAXS measurements of non-critical (A, B) and critical (C, D) femoral osteotomy samples at 2 and 6 weeks post-osteotomy, respectively. For every measurement point the mean mineral particle thickness (T parameter) is shown color-coded and the degree of orientation (ρ parameter) as well as the direction of the predominant orientation are given bar-coded (by length and orientation of the small black bars). (E–H) The predominant orientation of the mineral platelets within the tissue by arrows (as shown in higher resolution in (A–D) by direction of small black bars).

axis of the bone) (Fig. 4F), whereas the orientation within the closure of the C6 sample was also well aligned, but in a horizontal direction (perpendicular to the long axis) (Fig. 4H), following the curvature of the closure.

3.3.2. Degree of orientation

The cortex area had much higher ρ parameter values than the bony callus. For both models, the ρ was at ~0.4. For the first three time points (2–4 weeks), the values were higher, even more for the critical size osteotomy. The 6 week samples had slightly lower values (Tables 2 and 3). Taking these values as a reference for a mature bone, all the other areas for all the samples had considerably lower values. Within the periosteal callus of the non-critical healing model, the ρ parameter values near the osteotomy site mainly decreased or stayed approximately the same with increasing distance to the cortex (Table 2). For the periosteal callus far away from the osteotomy site, the ρ parameters values were in general higher than the values near the osteotomy and they stayed approximately the same while going outwards. For the N6 samples, this trend was also detected, and the ρ parameter values in the callus were generally higher. In the bony callus far away from the osteotomy gap of the N6I sample, the ρ values strongly increased with increasing distance to the cortex. The values for the area far away from the osteotomy almost reached the ρ values of the cortex, which were considered as the values of mature bone. For the critical size osteotomy model, the ρ parameter values in the periosteal callus near the osteotomy were higher than in the non-critical healing model. However, the increasing values at 6 weeks to almost cortical values cannot be observed (Table 3). With increasing distance to the osteotomy site, the ρ parameter values here rather decreased or stayed the same. Decreasing ρ parameter values in the periosteal callus with increasing distance to the cortex were seen in most cases, but there was also an exception. In summary, for the non-critical healing situation, the ρ parameter values increased with increasing distance to the osteotomy site and near the osteotomy they decreased with increasing distance to the cortex. In the non-critical healing model, the ρ parameter values increased between 4 and 6 weeks and almost reached the cortex state.

During non-critical healing, the endosteal callus had ρ parameter values in the same range as the periosteal callus. There were minimal differences with respect to the distance to the cortex, but in some cases we found increasing ρ parameter values with increasing distance (Table 2). However, for the later time points, there was less callus tissue and therefore fewer measurement points in the part far away from the osteotomy site, especially for the callus distant to the cortex. For the N6II sample, the values of the endosteal callus far away from the osteotomy almost reached the cortical values. However, the cortex values for this sample are comparably low. For the critical size osteotomy, with increasing distance to the endosteal cortex side (into the marrow cavity), the values mainly decreased. The endosteal callus far away from the osteotomy, deep in the medullary canal, had values strongly below the cortical values. The medullary closure in the critical size defects showed ρ parameter values of ~0.25–0.30 and they did not change over healing time. Summing up, for both models, ρ parameter values within the endosteal part were usually lower than in the cortex, and in the same range as in the periosteal callus, but there were no clear trends with increasing distance to the endosteal cortex or the osteotomy.

3.4. Mean mineral particle thickness

In the periosteal callus, the values usually increased with increasing distance to the cortex and sometimes reached values of ~2.2 nm. This phenomenon was seen in the early stages of the non-critical healing samples (Fig. 4A, red points) and in the later stages of the critical healing samples (Fig. 4D). Comparing the SAXS measurements with the ESEM/BSE images, the high T parameter values were mainly within the outer primary bone area, having a loose and not very compact morphology. For the endosteal callus, T parameter values were in the same range as in the cortex or slightly below. As there was no or only poorly mineralized tissue at the osteotomy site at 2 weeks post-osteotomy, there were no measurement results there, but a large mass of moderately mineralized tissue further away from the osteotomy was investigated (colored in blue and green, see Fig. 4A and C). For the N6 sample, the endosteal mineralized callus tissue was concentrated at the

Table 2
SAXS experiment results for non-critical healing samples.[a]

Parameter	Region	Samples						
		N2I	N2II	N3I	N3II	N4	N6I	N6II
ρ [–]	Cortex	0.41 ± 0.06	0.39 ± 0.07	0.41 ± 0.09	0.41 ± 0.06	0.43 ± 0.08	0.40 ± 0.07	0.36 ± 0.08
	B1	0.18 ± 0.09	0.27 ± 0.09	0.19 ± 0.07	0.17 ± 0.08	0.17 ± 0.07	0.26 ± 0.10	0.25 ± 0.10
	B2	0.10 ± 0.07	0.24 ± 0.11	0.14 ± 0.07	0.15 ± 0.07	0.18 ± 0.06	0.19 ± 0.13	0.23 ± 0.06
	A1	0.27 ± 0.06	0.26 ± 0.08	0.24 ± 0.05	0.27 ± 0.02	0.25 ± 0.10	0.32 ± 0.01	0.36 ± 0.05
	A2	0.25 ± 0.07	0.27 ± 0.07	0.25 ± 0.08	0.25 ± 0.06	0.26 ± 0.09	0.38 ± 0.02	0.34 ± 0.05
	B−1	0.21 ± 0.10	0.23 ± 0.04	0.19 ± 0.07	0.18 ± 0.06	0.16 ± 0.06	0.23 ± 0.10	0.24 ± 0.12
	B−2	0.20 ± 0.02	0.22 ± 0.07	0.17 ± 0.08	0.16 ± 0.07	0.14 ± 0.06	0.18 ± 0.08	0.30 ± 0.09
	A−1	0.21 ± 0.08	0.21 ± 0.06	0.24 ± 0.06	0.30 ± 0.09	0.16 ± 0.08		0.30 ± 0.04
	A−2	0.20 ± 0.06	0.21 ± 0.06	0.23 ± 0.07		0.08		0.31 ± 0.03
T [nm]	Cortex	1.9 ± 0.1	1.9 ± 0.1	2.0 ± 0.1	2.0 ± 0.1	2.0 ± 0.1	1.9 ± 0.1	2.0 ± 0.0
	B1	1.9 ± 0.1	1.9 ± 0.1	2.0 ± 0.1	2.0 ± 0.1	1.9 ± 0.1	1.9 ± 0.1	2.0 ± 0.1
	B2	2.1 ± 0.1	2.2 ± 0.1	2.1 ± 0.1	2.1 ± 0.1	1.9 ± 0.1	2.0 ± 0.1	2.0 ± 0.1
	A1	2.1 ± 0.2	2.0 ± 0.1	2.0 ± 0.0	2.0 ± 0.0	1.9 ± 0.1	1.9 ± 0.0	2.0 ± 0.1
	A2	2.2 ± 0.1	2.2 ± 0.1	2.1 ± 0.1	2.2 ± 0.1	2.0 ± 0.1	2.1 ± 0.1	2.1 ± 0.1
	B−1	1.8 ± 0.1	1.9 ± 0.1	1.9 ± 0.1	1.9 ± 0.1	1.9 ± 0.1	1.9 ± 0.1	2.0 ± 0.1
	B−2	1.8 ± 0.1	1.9 ± 0.1	1.8 ± 0.1	2.0 ± 0.1	1.9 ± 0.1	1.8 ± 0.1	2.0 ± 0.1
	A−1	1.9 ± 0.1	1.9 ± 0.1	2.0 ± 0.1	2.0 ± 0.1	2.0 ± 0.1		2.0 ± 0.0
	A−2	1.9 ± 0.1	1.9 ± 0.1	1.9 ± 0.0		1.9		1.8 ± 0.1

[a] Degree of orientation (ρ) and thickness of mineral particles (T) obtained by SAXS experiments with the laboratory X-ray scattering device. Measurements were performed for seven non-critical size osteotomy samples (two N2 and two N3 samples, one N4 sample and two N6 samples). ρ and T parameters were calculated for the seven samples and the measurement points were separated into nine areas (cortex as a reference, and periosteal and endosteal callus were divided into four subareas, near or far away from the osteotomy and adjacent to the cortex and the outer and inner part, respectively, see Fig. 1). For these nine areas, the parameters are given as mean values and standard deviation. The N2II, N4 and the N6II sample are shown in Fig. 2A–C and Fig. 4A and B shows the samples N2II and N6II.

Table 3
SAXS experiment results for critical healing samples.[a]

Parameter	Region	Samples							
		C2I	C2II	C3I	C3II	C4I	C4II	C6I	C6II
ρ [-]	Cortex	0.43 ± 0.06	0.42 ± 0.06	0.46 ± 0.07	0.42 ± 0.07	0.43 ± 0.06	0.44 ± 0.06	0.41 ± 0.05	0.36 ± 0.07
	B1	0.28 ± 0.03	0.34 ± 0.05	0.30 ± 0.10	0.28 ± 0.05	0.29 ± 0.04	0.39 ± 0.04	0.28 ± 0.08	0.25 ± 0.06
	B2		0.34 ± 0.03	0.22 ± 0.07		0.32 ± 0.07	0.33 ± 0.09		0.30 ± 0.08
	A1	0.33 ± 0.06	0.36 ± 0.07	0.29 ± 0.10	0.29 ± 0.06	0.29 ± 0.05	0.35 ± 0.03	0.23 ± 0.08	0.25 ± 0.08
	A2		0.33 ± 0.06	0.23 ± 0.13	0.32 ± 0.00	0.25 ± 0.08	0.25 ± 0.07	0.19 ± 0.08	0.26 ± 0.10
	B−1	0.25 ± 0.07	0.42 ± 0.06	0.29 ± 0.16	0.25 ± 0.05	0.27 ± 0.07	0.28 ± 0.07	0.23 ± 0.08	0.21 ± 0.06
	B−2	0.24 ± 0.08	0.28 ± 0.07	0.35 ± 0.15	0.19 ± 0.08	0.24 ± 0.09	0.23 ± 0.07	0.22 ± 0.08	0.21 ± 0.09
	A−1	0.29 ± 0.08	0.37 ± 0.09	0.35 ± 0.13	0.11	0.20 ± 0.07	0.34 ± 0.06	0.21 ± 0.06	0.19 ± 0.03
	A−2	0.19 ± 0.09	0.25 ± 0.05	0.25 ± 0.18	0.19 ± 0.11	0.24 ± 0.08	0.30 ± 0.08	0.24 ± 0.06	0.20 ± 0.01
	C	0.25 ± 0.05	0.29 ± 0.08	0.28 ± 0.20	0.26 ± 0.07	0.25 ± 0.05	0.28 ± 0.10	0.26 ± 0.06	0.26 ± 0.05
T [nm]	Cortex	1.9 ± 0.1	1.9 ± 0.1	2.0 ± 0.1	2.0 ± 0.1	1.9 ± 0.1	2.1 ± 0.1	1.9 ± 0.1	1.9 ± 0.1
	B1	2.0 ± 0.1	2.1 ± 0.0	2.2 ± 0.1	2.0 ± 0.1	2.0 ± 0.1	2.1 ± 0.1	2.0 ± 0.2	2.0 ± 0.1
	B2		2.0 ± 0.0	2.2 ± 0.1		2.1 ± 0.2	2.2 ± 0.0		2.0 ± 0.1
	A1	2.0 ± 0.1	1.9 ± 0.1	2.1 ± 0.1	2.0 ± 0.1	2.0 ± 0.1	2.1 ± 0.1	1.9 ± 0.1	2.0 ± 0.1
	A2		2.0 ± 0.1	2.1 ± 0.1	2.1 ± 0.0	2.1 ± 0.1	2.1 ± 0.1	2.1 ± 0.1	2.0 ± 0.1
	B−1	1.9 ± 0.1	1.9 ± 0.0	2.0 ± 0.1	1.9 ± 0.1	1.9 ± 0.1	2.0 ± 0.1	1.9 ± 0.1	1.9 ± 0.0
	B−2	2.0 ± 0.1	1.9 ± 0.1	1.9 ± 0.1	1.9 ± 0.0	1.9 ± 0.1	1.9 ± 0.0	1.9 ± 0.0	1.9 ± 0.1
	A−1	1.9 ± 0.0	1.9 ± 0.1	1.9 ± 0.1	1.8	1.9 ± 0.1	2.0 ± 0.1	1.8 ± 0.0	1.9 ± 0.0
	A−2	1.8 ± 0.0	1.8 ± 0.0	2.0 ± 0.1	1.9 ± 0.1	1.9 ± 0.1	2.0 ± 0.1	1.9 ± 0.1	2.0 ± 0.0
	C	2.0 ± 0.1	1.9 ± 0.1	2.1 ± 0.1	2.0 ± 0.1	2.1 ± 0.1	2.1 ± 0.1	2.0 ± 0.1	2.0 ± 0.1

[a] Degree of orientation (ρ) and thickness of mineral particles (T) obtained by SAXS experiments with the laboratory X-ray device. Eight critical healing samples were analyzed (two C2, two C3, two C4 and two C6 samples). The different areas are the same as in Table 2, and there is an additional tenth area (closure). ρ and T parameters are given for these areas as mean and standard deviation. The C2II, the C4II, and the C6II sample are presented in Fig. 2D–F and C2II and C6II in Fig. 4C and D.

osteotomy site and had T parameter values in the range of the cortex values (in green and yellow color, Fig. 4B), whereas for the C6 sample a dense closure of the marrow cavity was detected, also having T parameter values in the cortical range.

These results were confirmed quantitatively by calculating mean values and standard deviations (Tables 2 and 3). Compared to the mean values of the cortex of 1.9–2.0 nm in non-critical osteotomies (Table 2) and except for one sample also in critical size defect (Table 3), the values of the periosteal callus were equal or higher, for all the time points and both healing models. The non-critical healing model showed the highest T parameter values for the outer periosteal callus far away from the osteotomy (Table 2). Within the periosteal callus, T parameter values increased with increasing distance to the cortex. In these two samples, also an increase in T parameter values with increasing distance to the osteotomy was detected, but for the other samples, this trend was only true for the outer part of the callus. This also shows that even at the latest time point, we still had very high T parameter values remaining for the outer periosteal callus, far away from the osteotomy, whereas the other periosteal areas had values equal to the cortex. During these 6 weeks of healing, the T parameter decreased for the outer periosteal callus near the osteotomy; as for the earlier time points, this area still had higher values compared to the cortex. In the periosteal callus adjacent to the cortex, the T parameter values were similar to the cortex. For the critical size osteotomy, most of these findings were also true. With increasing distance to the periosteal cortex, T parameter values mainly increased, even for the later time points (Table 3). However, the highest values for the critical size osteotomy model were in the outer periosteal callus near the osteotomy. Therefore, the T parameter values rather decreased with increasing distance to the osteotomy site. To sum up, T parameter values were the same or higher than in the cortex, and had their maximal values in the outer periosteal callus part. For the non-critical healing, the highest values were farther away from the osteotomy site than in the critical size osteotomy model. Mineral particle thickness increased with increasing distance to the periosteal cortex, for both models; however, with increasing distance to the osteotomy T values in the outer periosteal callus part of the non-critical healing model increased, but decreased for the critical size osteotomy model.

The endosteal callus part had values slightly below the cortical T parameter values, for both the non-critical healing and the critical size osteotomy model and the lowest values were in the endosteal callus near the osteotomy for the non-critical and far away from the osteotomy for the critical size model (Tables 2 and 3). The values for the endosteal callus adjacent to the cortex and far away from the osteotomy of the non-critical healing model were quite high at the later time points. Again, the values increased for the non-critical healing in the adjacent endosteal callus with increasing distance to the osteotomy, whereas the values were decreasing for the critical size osteotomy. The closures in the C2 samples were in the cortical range, but were higher than that at the other time points.

3.5. Gradients in particle orientation, mean crystal length and mean particle thickness in high resolution

To analyze gradients within the callus tissue structure, we used a synchrotron source to scan large areas with higher resolution. The cortical bone tissue was highly oriented in a vertical direction (parallel to the long axis of the bone, Fig. 5A, lower part of the vertical area) and it had T parameter values of 1.8–1.9 nm (blue green). L parameter values were at ∼20–22 nm (green, Fig. 5B). The upper half of the vertical area showed the newly formed callus tissue within the osteotomy gap. Also there, two different types of callus, a rather loose and poorly structured primary bone in the outer part and a more compact, and lamellar structured secondary bone in the inner part, were found. Both had lower ρ parameter values than the cortical region and the mineral platelets were oriented perpendicular to the axis of the long bone within the gap and turning downwards in a diagonal direction around the remaining cortex.

Looking at the T parameter, the callus near the cortex still had values of ∼2.0–2.1 nm (light green), so slightly above the cortical ones. With increasing distance to the remaining cortex, the values further increased and reached values of 2.3–2.4 nm (orange red). At the same time, L parameter values decreased and reached values of ∼16 nm (blue). The horizontal area started in the lamellar structured callus, adjacent to the cortex, and ended in the very loose outer callus (Fig. 5). Similar to the results shown in Fig. 4D and in Table 2 (N6II), the T parameter values increased with increasing
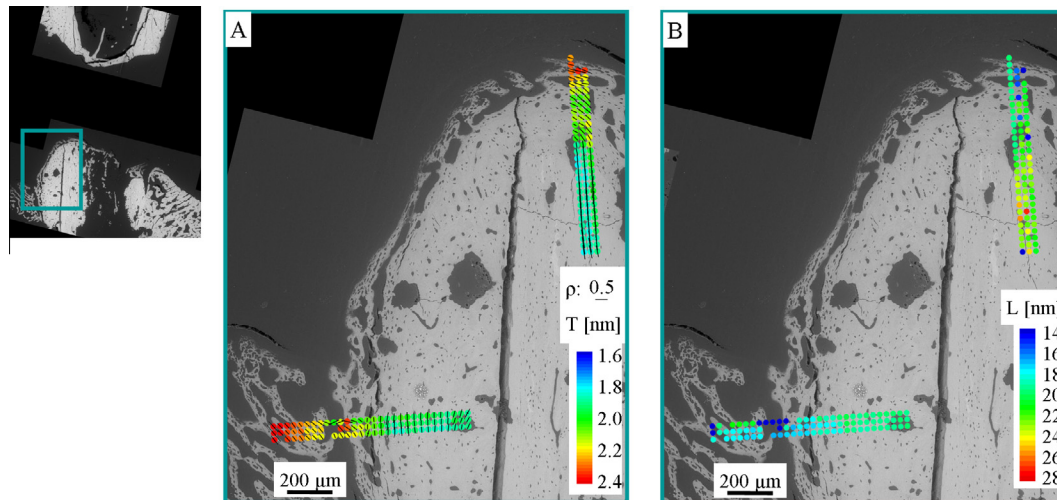
Fig. 5. High resolution scanning synchrotron X-ray scattering experiments performed on the same sample as in Fig. 4D. (A) The degree of orientation (ρ parameter) and predominant orientation are given as length and direction of black bars, the mean particle thickness (T parameter) is given color-coded. (B) The mean crystal length (L) is given in color-coded.

distance to the cortex from values of 1.9 nm (blue green) to 2.4 nm or even higher (red). The adjacent callus part already reached values similar to the cortex, whereas the values for the outer part still remained very high. Also, L parameter values decreased and reached values of ∼16 nm (blue) in the outer periosteal callus. Looking at the ρ parameter, these values decreased with increasing distance to the cortex, meaning that the degree of orientation of the mineral platelets became smaller. Also in the direction of the predominant orientation, changes were detectable. The adjacent part was oriented inwards, forming a bow towards the cortex and the osteotomy gap. The middle part of the compact callus was oriented parallel to the cortex and the long axis of the bone and within the outer loose callus part the orientation went outwards in a diagonal direction.

4. Discussion

The current study analyzed bony callus structure and properties at several levels of hierarchy to explore the influence of the mechanical environment resulting from different geometrical conditions, namely differing gap sizes. Our results showed that bone healing in non-critical and critical size osteotomies is in principle similar, but the tissues are arranged distinctly differently. In particular, we found the following similar phenomena: (i) primary bone formation was followed by secondary bone deposition; (ii) particle dimensions changed during deposition and growth, from on average short and thick to long and thin particles; and (iii) gradients of mechanical properties across cortex and callus. At the time when bony bridging occurred in non-critical healing (between 4 and 6 weeks post-osteotomy), nanostructure and microstructure developed towards the original ordered structure of cortical bone. We found three main differences between the two cases. In non-critical healing samples we discovered (iv) a shell-like structured callus containing large marrow-filled holes, (v) bony bridging at first in the endosteal callus and (vi) a process of reorientation within the callus. In the critical healing situation, the periosteal and endosteal callus did not bridge and the orientation of the tissue was notably different from both the cortex and the non-critical healing situation.

4.1. Influence of mechanical environment on cells and tissue formation

The mechanical conditions at the fracture site are linked across different organizational levels: organ, tissue and cell level [9,11].

Thus, stress and strain at the organ and tissue level can be sensed by single cells, influencing cell proliferation and differentiation [11]. In addition, the local tissue properties, such as stiffness, around the cells influence cell behavior [10]. It is thought that the magnitude of stress and strain at the fracture gap drives cell differentiation and proliferation [11,12]. In our study, cells embedded in the soft tissue likely sense different mechanical stimuli as a function of the gap size. This might promote vascularization and enhance both intramembranous and endochondral bone formation in the non-critical case, which is lacking in the critical case [11]. In the non-critical case, ossification proceeds and finally the gap is bridged.

4.2. Primary bone formation and secondary bone deposition

At 2 weeks post-osteotomy, the fragments had already become occupied with periosteal and endosteal callus. This primary bone callus had a very loose appearance, with many small holes, and it was only partly mineralized. The very loose and poorly ordered structure is similar to the woven bone previously characterized in sheep [8]. In both the endosteal and periosteal callus region, osteotomy fragments were still separated by a gap consisting of cartilage tissue (Fig. S.2A). Calcification and mineralization occurred and bone was formed via endochondral ossification [4]. With progressing healing, the endosteal and periosteal callus became denser and concentrated at the osteotomy site. The callus had a more compact, already remodeled structure and could be described as lamellar. In terms of mineral particle orientation (Fig. 2A and D), non-critical and critical healing samples initially resembled each other. An outwards orientation of the mineral platelets within the periosteal callus tissue was detected although this area was poorly ordered compared to cortical bone. Even in the later time points of critical healing, the outer part of the periosteal callus tissue still showed a primary bone appearance and an outwards reaching orientation. Thus for the early phases of healing we can state that non-critical and critical healing seemed to progress via the same steps.

4.3. Changes in mineral particle dimensions

Mineralization processes leave fingerprints in the form of mineral particle properties in bone tissue. A spatial analysis of mineral properties across selected sample regions enabled a temporal interpretation of the mineralization processes. Mineralization of

the collagen matrix during remodeling proceeds in two phases [13]: a quick primary one, mineralizing up to 70% to the total capacitance within a few days with particles growing two-dimensionally, an increase in specific particle surface and a slow secondary one proceeding with increasing particle thickness [13]. Whether transient precursors like amorphous calcium phosphates were involved [26,27], or rather small biological apatite particles increasing in size and crystallinity were directly formed, is still unclear [28]. However, in our study, all measured points showed a (002) peak, indicating crystalline hydroxyapatite at the time of investigation. Relatively thick mineral particles (Fig. 4A and D, outer periosteal callus, colored in red) were found within the loose primary bone tissue, which corresponded presumably to a younger, more recently formed tissue. The mineral platelets showed a decrease of mean thickness over time, which was concluded from decreasing T parameter values towards the inner callus regions. In younger tissue, the mean particle thickness was larger compared to the older one, whereas the mean length was smaller. A similar finding was described during normal bone growth by Lange et al., investigating fetal and postnatal particle size in mice [24]. The authors concluded that there were first particles present within the bone, having a short and bulky shape, showing a poor alignment. The particles then gained in length and became better aligned. However, the mean particle thickness also grew, whereas in our study, the mean particle thickness was even smaller in the older tissue. This was probably due to few thick particles in the primary bone that either were removed and replaced by thinner particles in the secondary bone or remained but were surrounded by many additionally deposited thin particles which then led to a decreased mean particle thickness.

4.4. Gradients of mechanical properties

The mechanical properties for the cortex were not uniform. Shipov et al. recently demonstrated that in cortical rat bone different regions with different mechanical, compositional, and structural properties could be distinguished, namely the circumferential lamellar bone at the endosteal and/or periosteal part and a disorganized bone region in between [29]. This is in accordance with the fact that also the cortices of long bones in mice were not homogenously structured [29,30]. They had a poorly ordered bone structure in the center, and only the outer parts at the endosteal and periosteal edge of the cortex showed a remodeled lamellar structure. However, in contrast to our results, where the outer parts of the cortex, within this lamellar structured area, had higher values, Shipov et al. reported lower values of the indentation modulus for these outer regions [29]. We explained this by the fact that this lamellar bone was anisotropically structured and we used longitudinal sections for the indentation experiments, whereas the reported study was performed on transversal sections. In the periosteal callus, hardness and indentation modulus increased with increasing distance to the osteotomy site, and for the non-critical healing, the lowest values were found within the osteotomy gap. However, as only the 6 week samples have been analyzed, and there was a normal biological variety between the individual animals, more samples have to be analyzed to determine if there exists a general trend in healing. As cortical rat bones show no or hardly any remodeling and are separated into two structurally different parts, they have crucial differences in their structure compared to human bones, which raises the question whether rat and mouse are adequate animal models for studying human bone diseases [29].

4.5. Shell-like callus structure

At 4–6 weeks post-osteotomy, the presence of a shell-like structured callus was one remarkable difference between the non-critical and critical size osteotomy. In both healing situations, endosteal and periosteal callus became denser and concentrated at the osteotomy site, but only for non-critical healing did we see that the periosteal callus was built up in a shell-like structure with large holes adjacent to the original cortices (Fig. S.1B and C). This structure bridged the osteotomy gap and probably improved the mechanical properties of the osteotomy. As already suggested by Carter et al., bony bridging probably transmitted higher loads across the gap and kept it away from the still fragile inner parts [11]. In our model (Fig. S.1), we suggest that even in the later time points, the tissue within the osteotomy gap was not yet able to bear high loads, and the outer shell of the mineralized callus tissue transmitted them towards the other side of the osteotomy. At the same time it presumably allowed loads of a certain degree to stimulate remodeling. The critical healing samples lacked the formation of such a shell-like structure, including the marrow-filled holes. Probably no load transfer was possible because of a large gap filled with non-mineralized tissue that did not give further stability. First signs of bone resorption at the preexisting cortex (Fig. 2F, R) were visible, which is in accordance with previous findings [16] where the rounding of the cortical ends by resorption was described.

4.6. Bony bridging of the fracture gap

Presumably the most important difference between the two healing processes is the development of a bony bridging during non-critical healing. In our study it occurred at the endosteal side first. In contrast, during critical healing, the periosteal callus of the opposing osteotomy ends was not in contact, and seldom grew further then the edge of the remaining cortex. The endosteal callus deeply penetrated into the osteotomy gap, reaching out for the opposite side. By forming an arc-shaped bony closure of the marrow cavity the endosteal callus formation led to a narrowing of the osteotomy gap, which has already been described [15,16]. Marsh distinguishes between periosteal, rapid endosteal and slow endosteal healing in human fracture healing [31]. He states that after failing of these two rapid bridging mechanisms (periosteal and rapid endosteal), late bridging of the fracture during slow endosteal healing is possible via the formation of an intramedullary bony callus [31]. In the critical healing part of our study, the formation of the endosteal callus, reaching towards the opposing osteotomy fragment, possibly was the end of the rapid endosteal and the beginning of the slow endosteal healing response. However, similar to previously described cases [15,16], the endosteal callus was not able to bridge the osteotomy gap and healing failed.

4.7. Reorientation processes within the callus

During the formation of this shell-like structure and the building of a bony bridging a reorientation of the nanostructure within the callus took place. The initial orientation of the mineral platelets (Fig. 4A and E) pointed towards the outer side of the osteotomy. At a later time point their orientation followed a bow turning into the osteotomy, just along the non-mineralized contact line (medial periosteal callus in Figs. 2C, S.2C and Fig. 4B and F). As soon as the gap was bridged, the orientation changed once more and led distal to proximal, across the osteotomy towards the opposing cortex end (endosteal callus, Figs. 2C, S.2F and Fig. 4B and F). During critical healing, this reorientation only partly happened. In particular, as bridging never occurred the arc-like shaped closure showed lateral to medial orientation, following the curvature of the arc.
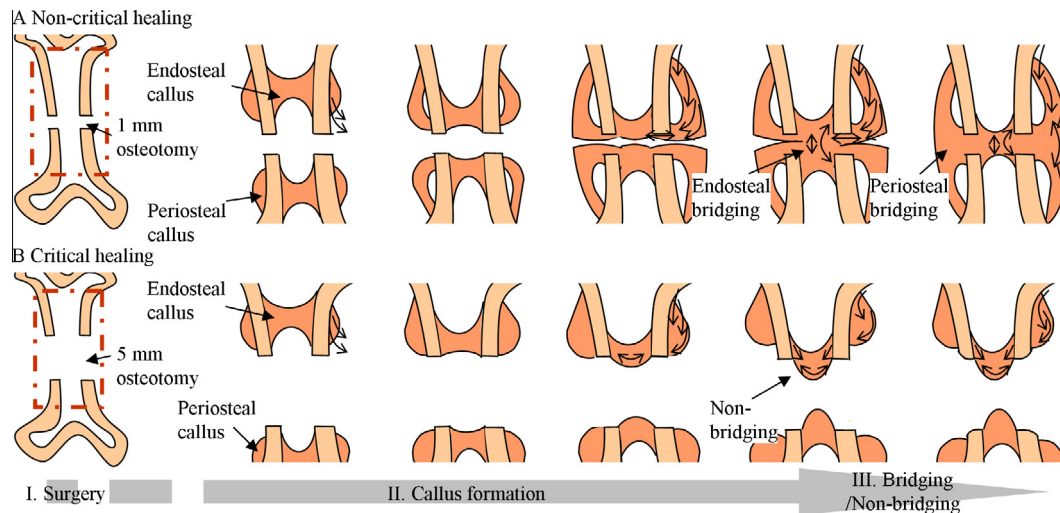
Fig. 6. Model of healing in a non-critical (A) and a critical (B) healing situation. After first loose bone callus formation, the tissue was remodeled and big holes became visible (stage II, callus formation). The crucial point was stage III, bridging/non-bridging, where at first the endosteal callus fused to form a bony bridge. The mechanical situation for the non-critical healing model is completely changed and a reorientation of the bone callus tissue took place, whereas in the critical healing situation the lack of these mechanical changes led to a closure of the marrow cavity.

5. Conclusion

In conclusion, the compositional, structural and mechanical changes in the callus tissue followed the same consecutive steps during non-critical and critical size osteotomy healing. In both processes, initially large volumes of poorly organized and weakly mineralized endosteal and periosteal callus were formed (Fig. 6, stage I). Both the endosteal and the periosteal callus of the opposing osteotomy ends proceeded towards bony bridging of the osteotomy gap. In both healing situations, the marrow cavity was closed off by endosteal callus. In the non-critical healing process the two callus parts were separated by a small non-mineralized line (cartilage tissue, see Fig. S.2B and C) that was bridged during advanced healing. After this bridging, the mechanical situation was completely changed and a reorientation of the tissue was initiated. Thus, the crucial point of healing was the bony bridging of the gap and in turn the union of the opposing callus parts (Fig. 6, stage III). In our non-critical healing samples, the endosteal bridging occurred before periosteal bridging. Due to the improved transmission of load by the achieved bridging, healing could be completed by starting the resorption of the surplus callus tissue and proceeded towards a bone with totally restored shape and function. In contrast, in the critical size osteotomy this switching of the mechanical environment never happened; the bone did not undergo such a restructuring and reorientation. Instead, the closure of the marrow cavity was established and rounding of the cortices occurred. The differentiation between the two healing processes occurred between 4 and 6 weeks post-osteotomy. The varied geometrical conditions in critical and non-critical healing induce completely different mechanical situations responsible for the outcome of healing.

Disclosures

All authors state that they have no conflicts of interest.

Acknowledgments

Appendix A. Figures with essential color discrimination

Certain figures in this article, particularly Figs. 1 and 6 are difficult to interpret in black and white. The full color images can be found in the on-line version, at http://dx.doi.org/10.1016/j.actbio.2014.05.023.

Appendix B. Supplementary data

Supplementary data associated with this article can be found, in the online version, at http://dx.doi.org/10.1016/j.actbio.2014.06.003.

References

[1] Fratzl P, Weinkamer R. Nature's hierarchical materials. Prog Mater Sci 2007;52:1263–334.
[2] Frost HM. A 2003 update of bone physiology and Wolff's Law for clinicians. Angle Orthod 2004;74:3–15.
[3] Calori GM, Mazza E, Colombo M, Ripamonti C. The use of bone-graft substitutes in large bone defects: any specific needs? Injury 2011;42:S56–63.
[4] Shapiro F. Bone development and its relation to fracture repair. The role of mesenchymal osteoblasts and surface osteoblasts. Eur Cell Mater 2008;15:53–76.
[5] Einhorn TA. The cell and molecular biology of fracture healing. Clin Orthop Relat R 1998;355:S7–S21.
[6] Dimitriou R, Tsiridis E, Giannoudis PV. Current concepts of molecular aspects of bone healing. Injury 2005;36:1392–404.
[7] Doll B, Aleef M, Hollinger JO. Overview of fracture repair. In: Pietrzak WS, editor. Musculoskeletal tissue regeneration: biological materials and methods. New York: Humana Press; 2008. p. 39–61.
[8] Liu YF, Manjubala I, Schell H, Epari DR, Roschger P, Duda GN, et al. Size and habit of mineral particles in bone and mineralized callus during bone healing in sheep. J Bone Miner Res 2010;25:2029–38.
[9] Epari DR, Duda GN, Thompson MS. Mechanobiology of bone healing and regeneration: in vivo models. Proc Inst Mech Eng H 2010;224(H12):1543–53.
[10] Discher DE, Janmey P, Wang YL. Tissue cells feel and respond to the stiffness of their substrate. Science 2005;310(5751):1139–43.
[11] Carter DR, Beaupre GS, Giori NJ, Helms JA. Mechanobiology of skeletal regeneration. Clin Orthop Relat R 1998;355:S41–55.

[12] Claes LE, Heigele CA. Magnitudes of local stress and strain along bony surfaces predict the course and type of fracture healing. J Biomech 1999;32:255–66.

[13] Fratzl P, Gupta HS, Paschalis EP, Roschger P. Structure and mechanical quality of the collagen-mineral nano-composite in bone. J Mater Chem 2004;14:2115–23.

[14] Weiner S, Wagner HD. The material bone: structure mechanical function relations. Annu Rev Mater Sci 1998;28:271–98.

[15] Mehta M, Schell H, Schwarz C, Peters A, Schmidt-Bleek K, Ellinghaus A, et al. A 5-mm femoral defect in female but not in male rats leads to a reproducible atrophic non-union. Arch Orthop Trauma Surg 2011;131:121–9.

[16] Mehta M, Checa S, Lienau J, Hutmacher D, Duda GN. In vivo tracking of segmental bone defect healing reveals that callus patterning is related to early mechanical stimuli. Eur Cell Mater 2012;24:358–71.

[17] Schwarz C, Wulsten D, Ellinghaus A, Lienau J, Willie BM, Duda GN. Mechanical load modulates the stimulatory effect of BMP2 in a rat nonunion model. Tissue Eng A 2013;19:247–54.

[18] Roschger P, Gupta HS, Berzlanovich A, Ittner G, Dempster DW, Fratzl P, et al. Constant mineralization density distribution in cancellous human bone. Bone 2003;32:316–23.

[19] Manjubala I, Liu Y, Epari DR, Roschger P, Schell H, Fratzl P, et al. Spatial and temporal variations of mechanical properties and mineral content of the external callus during bone healing. Bone 2009;45:185–92.

[20] Fratzl P. Statistical model of the habit and arrangement of mineral crystals in the collagen of bone. J Stat Phys 1994 Oct;77(1–2):125–43.

[21] Rinnerthaler S, Roschger P, Jakob HF, Nader A, Klaushofer K, Fratzl P. Scanning small angle X-ray scattering analysis of human bone sections. Calcif Tissue Int 1999;64:422–9.

[22] Klug HP, Alexander LE. X-ray diffraction procedures for polycrystalline and amorphous materials. 2nd ed. New York: Wiley; 1974.

[23] Pabisch S, Wagermaier W, Zander T, Li C, Fratzl P. Imaging the nanostructure of bone and dentin through small- and wide-angle X-ray scattering. Methods Enzymol 2013;532:391–413.

[24] Lange C, Li C, Manjubala I, Wagermaier W, Kühnisch J, Kolanczyk M, et al. Fetal and postnatal mouse bone tissue contains more calcium than is present in hydroxyapatite. J Struct Biol 2011;176:159–67.

[25] Danilchenko SN, Kukharenko OG, Moseke C, Protsenko IY, Sukhodub LF, Sulkio-Cleff B. Determination of the bone mineral crystallite size and lattice strain from diffraction line broadening. Cryst Res Technol 2002;37:1234–40.

[26] Nudelman F, Pieterse K, George A, Bohmans PHH, Friedrich H, Brylka LJ, et al. The role of collagen in bone apatite formation in the presence of hydroxyapatite nucleation inhibitors. Nat Mater 2010;9:1004–9.

[27] Weiner S. Transient precursor strategy in mineral formation of bone. Bone 2006;39:431–3.

[28] Grynpas MD. Transient precursor strategy or very small biological apatite crystals? Bone 2007;41:162–4.

[29] Shipov A, Zaslansky P, Riesemeier H, Segev G, Atkins A, Shahar R. Unremodeled endochondral bone is a major architectural component of the cortical bone of the rat (*Rattus norvegicus*). J Struct Biol 2013;183:132–40.

[30] Kerschnitzki M, Wagermaier W, Roschger P, Seto J, Shahar R, Duda GN, et al. The organization of the osteocyte network mirrors the extracellular matrix orientation in bone. J Struct Biol 2011;48:303–11.

[31] Marsh D. Concepts of fracture union, delayed union, and nonunion. Clin Orthop Relat R 1998;355:S22–30.